Supplementary Materials: Solution-Processed Environmentally Friendly Ag_2S Colloidal Quantum Dot Solar Cells with Broad Spectral Absorption

Viktor A. Öberg, Xiaoliang Zhang, Malin B. Johansson and Erik M. J. Johansson *

Two different linkers were tested during the experiments: 3-mercaptopropionic acid (3-MPA) and ethanedithiol (EDT). Experiments showed that 3-MPA did not work in making films with the as-synthesized Ag_2S CQDs. Further experiments in which 3-MPA and acetic acid was added to a 2-phase system with the dodecanethiol-capped Ag_2S CQDs in cyclohexane and dimethylformamide showed that systems with 3-MPA swapped phases while acetic acid did not. This showed that there is an exchanged between the thiol groups, but not between the thiol and carboxylic acid. This means that 3-MPA substitutes the dodecanethiol ligands, but cannot act as a linker because the carboxylic acid is not reactive towards the Ag-S-bond on the surface of the CQDs. Compared to 3-MPA, EDT worked as a linker as the film thickness grew thicker with each layer, resulting in a flat film thicker than 100 nm.

The two HTMs that are investigated in this study are poly(3-hexylthiophene-2,5-diyl) (P3HT) and spiro-OMeTAD. Both of these materials have been used extensively in many different solar cell devices ranging from polymer solar cells, hybrid perovskite solar cells to quantum dot solar cells[1-8]. P3HT has been reported to have its highest occupied molecular orbital (HOMO) and lowest unoccupied molecular orbital (LUMO) levels at -5.1 and -2.9 eV respectively[4,9], while spiro-OMeTAD has its HOMO level at -5.22[10]. The P3HT in this study was undoped, while spiro-OMeTAD was doped with cobalt and lithium according to previous studies to lower the Fermi level and increase the conductivity[11]:

For 300 μL spiro-OMeTAD solution (70 mM):

Prepare 0.26 g t-BP in 10 mL chlorobenzene (ca 0.2 M).

Add 25.74 mg spiro-OMeTAD (21 μmol) in 272 μL t-BP solution.

Prepare 0.6 M LiTFSI in acetonitrile (e.g. 27.22 mg in 100 μL acetonitrile.)

Prepare Co-complex by adding 10 mg to 300 μL acetonitrile.

Add 21 μL LiTFSI solution and ca 6.6 μL Co solution to the spiro-OMeTAD solution.

The solution was then spin-coated as is on top of QD films.

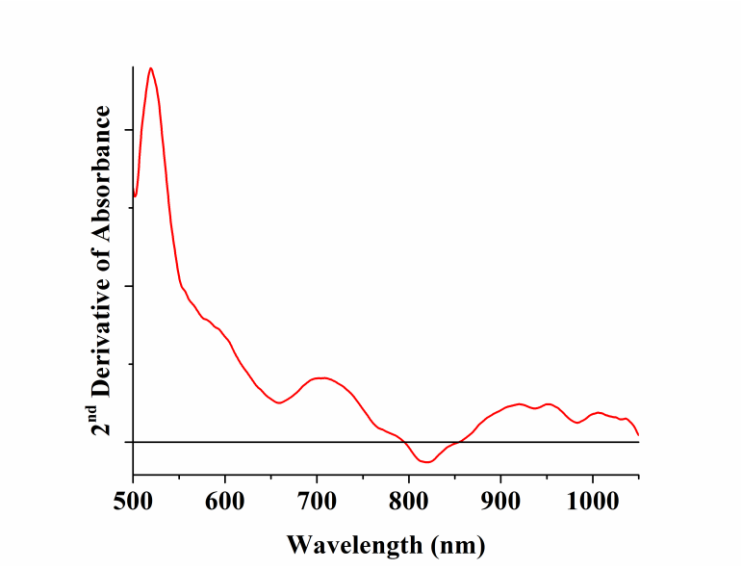

Figure S1. 2nd derivative of the absorbance spectrum for a CQD dispersion with a concentration of 2 mg/mL. There is a range between 795 and 855 nm (negative values) with a peak at 820 nm corresponding to a shoulder/ hidden peak in the absorption spectrum. The spectrum has been smoothed using Savitzky-Golay with a point window of 100.

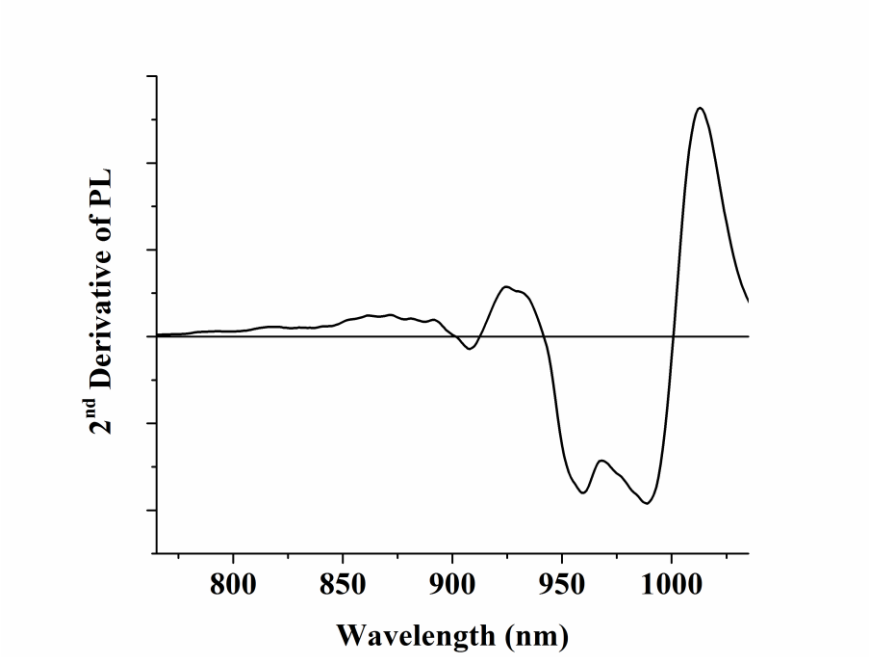

Figure S2. 2nd derivative of the PL spectrum seen in Figure 1(a). There is a range between 902 and 912 nm (negative values) with a peak at 908 nm corresponding to a shoulder/ hidden peak in the PL spectrum. The spectrum has been smoothed using Savitzky-Golay with a point window of 10.

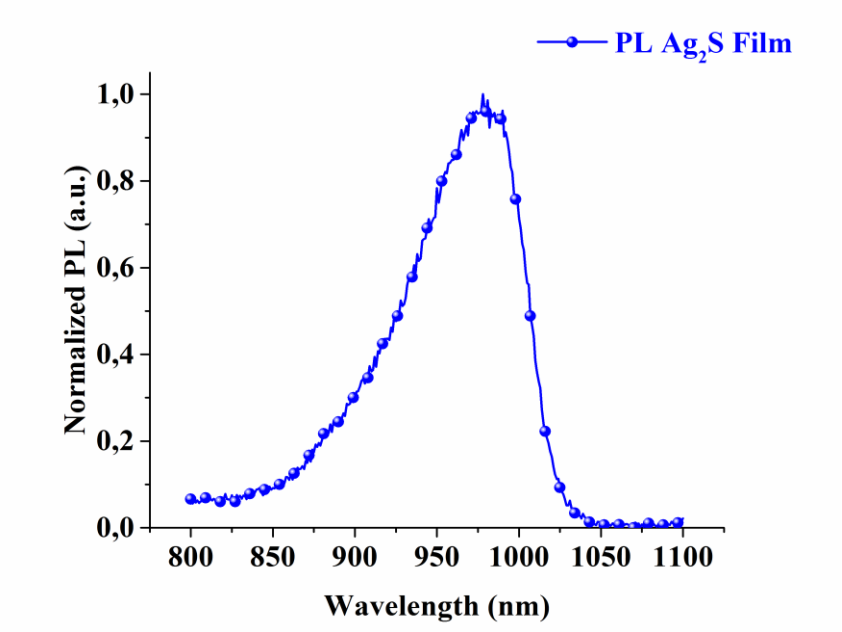

Figure S3. Normalized PL emission spectrum of a thin layer of Ag_2S film. The Ag_2S QDs are still protected by their dodecanethiol ligand, and thus they show a similar PL spectrum as the dispersion.

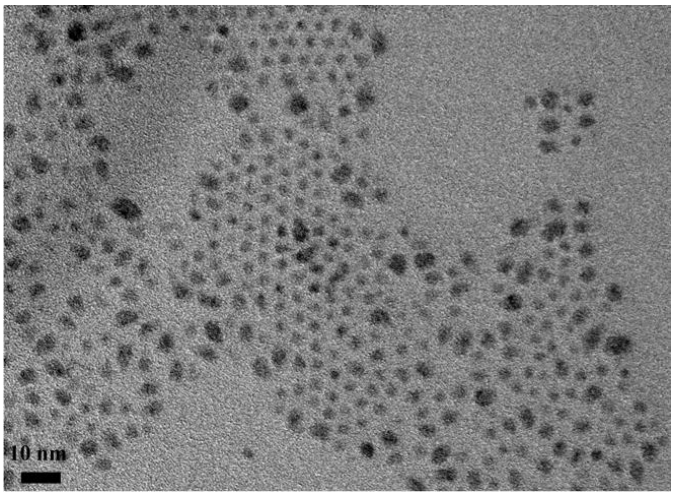

Figure S4. TEM image from which S5 (below) is based on.

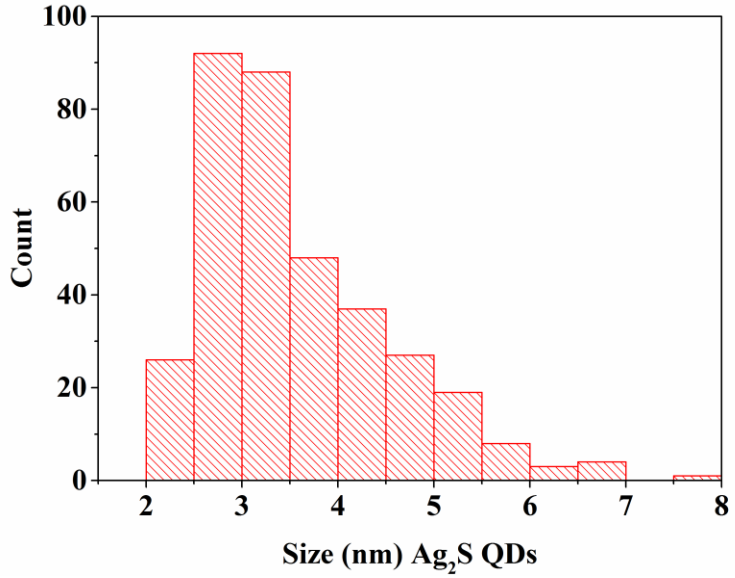

Figure S5. Size distribution of the Ag_2S quantum dots. Average size: 3.59 nm. Sample standard deviation, σ: 0.97 nm. The parameters were calculated using the TEM image seen in Figure S4.

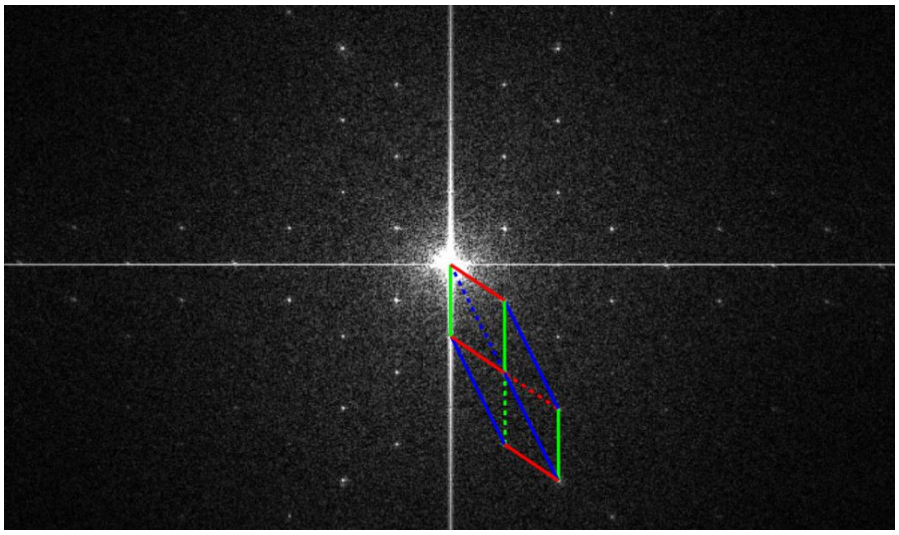

Figure S6. FFT pattern of 1 single quantum dot crystal showing that it is monocrystalline. In the figure is a proposed position of the reciprocal lattices a*, b* and c*. Note that it is only the relative distances and directions of the reciprocal constants that are marked.

In Figure S5, a fast Fourier transform (FFT) can be seen for one of the quantum dots, showing it is monocrystalline in nature. The ratios of the absolute values of the proposed reciprocal lattices $\frac{|a^*|}{|b^*|}$, $\frac{|b^*|}{|c^*|}$ and $\frac{|a^*|}{|c^*|}$ matches well with the reciprocal lattices calculated from the real space lattices from a previous study on Ag_2S[12]:

$$\vec{a} = \begin{bmatrix} sin\beta * |a| \\ 0 \\ -cos\beta * |a| \end{bmatrix} \text{Å} = \begin{bmatrix} 4.1709 \\ 0 \\ 0.7042 \end{bmatrix} \text{Å}, \vec{b} = \begin{bmatrix} 0 \\ 6{,}91 \\ 0 \end{bmatrix} \text{Å}, \vec{c} = \begin{bmatrix} 0 \\ 0 \\ 7.87 \end{bmatrix} \text{Å};\ |a| = 4.23\ \text{Å}, \beta = 99.583°$$

$$\overrightarrow{a^*} = \frac{\vec{b} \times \vec{c}}{J} \text{Å}^{-1} = \begin{bmatrix} 0 \\ 6{,}91 \\ 0 \end{bmatrix} \times \begin{bmatrix} 0 \\ 0 \\ 7.87 \end{bmatrix} * J^{-1}\ \text{Å}^{-1} = \begin{bmatrix} 54.3817 \\ 0 \\ 0 \end{bmatrix} * J^{-1}\ \text{Å}^{-1}; J = \frac{V}{2\pi}\ \text{Å}^3$$

$$\overrightarrow{b^*} = \frac{\vec{c} \times \vec{a}}{J} \text{Å}^{-1} = \begin{bmatrix} 0 \\ 0 \\ 7.87 \end{bmatrix} \times \begin{bmatrix} 4.1709 \\ 0 \\ 0.7042 \end{bmatrix} * J^{-1}\ \text{Å}^{-1} = \begin{bmatrix} 0 \\ 32.849 \\ 0 \end{bmatrix} * J^{-1}\ \text{Å}^{-1}; J = \frac{V}{2\pi}\ \text{Å}^3$$

$$\overrightarrow{c^*} = \frac{\vec{a} \times \vec{b}}{J}\ \text{Å}^{-1} = \begin{bmatrix}4.1709\\0\\0.7042\end{bmatrix} \times \begin{bmatrix}0\\6.91\\0\end{bmatrix} * J^{-1}\ \text{Å}^{-1} = \begin{bmatrix}-4.886\\0\\28.8209\end{bmatrix} * J^{-1}\ \text{Å}^{-1}; J = \frac{V}{2\pi}\text{Å}^3$$

$$\rightarrow \left|\overrightarrow{a^*}\right| = 54.3817 * J^{-1}\ \text{Å}^{-1};\ \left|\overrightarrow{b^*}\right| = 32.849 * J^{-1}\ \text{Å}^{-1};\ \left|\overrightarrow{c^*}\right| = 29{,}2321\ * J^{-1}\ \text{Å}^{-1}$$

Table S1. Comparison between this study's ratios of the reciprocal lattice constants and a previous study's ratios of the reciprocal lattice constants calculated above.

	From previous study[12]	Calculated from Figure S5
$\frac{\lvert\boldsymbol{a}^*\rvert}{\lvert\boldsymbol{b}^*\rvert}$	1.6555	1.6665
$\frac{\lvert\boldsymbol{b}^*\rvert}{\lvert\boldsymbol{c}^*\rvert}$	1.1238	1.1165
$\frac{\lvert\boldsymbol{a}^*\rvert}{\lvert\boldsymbol{c}^*\rvert}$	1.8605	1.8606

Two distances in the planes in the crystal in the inset in Figure S6 were measured to be 0.226 nm and 0.264 nm respectively. Using Bragg's law gives 2θ = 39.84° and 33.92° respectively, matching peaks in the theoretical diffractogram in S7.

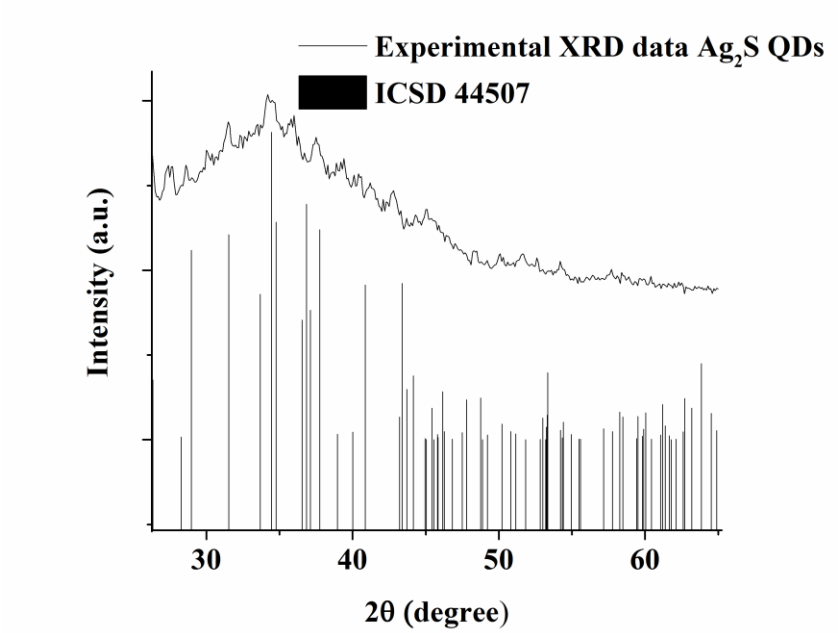

Figure S7. Experimental X-ray diffractogram of a thick drop-casted Ag_2S nanocrystal film as compared to a standard theoretical XRD spectrum ICSD 44507. As seen, only the overall shape of the spectrum is similar and comparable between the two, due to shape broadening of peaks due the small particles.

A third hole conductor, poly((2,3-bis(3-octyloxyphenyl)-5,8-quinoxalinediyl)-2,5-thiophenediyl) (TQ1), was also investigated in this study, as it has been shown to take a similar role as P3HT in organic polymer solar cells[13]. However, using TQ1 did not result in any comparable voltage and thus no efficiency was measured (see Figure S6).

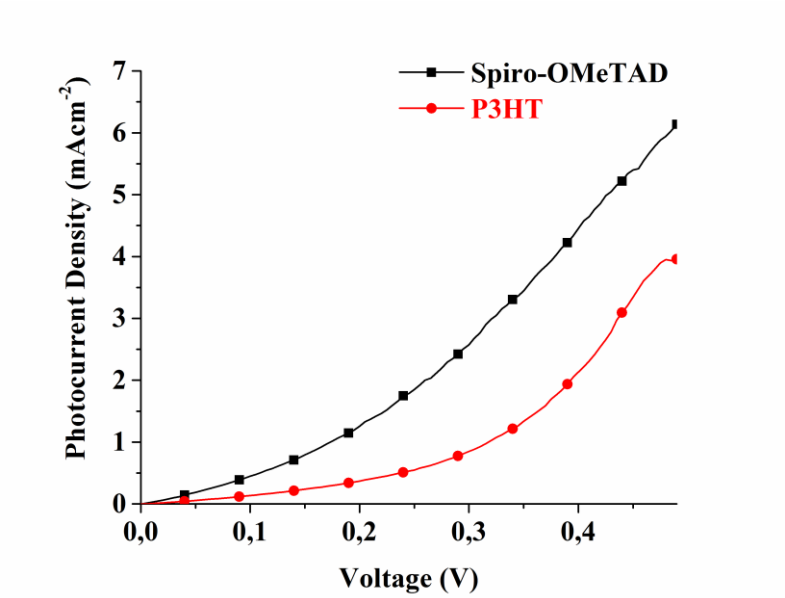

Figure S8. J-V curves of P3HT and spiro-OMeTAD cells in the dark. P3HT has a lower dark current than spiro-OMeTAD.

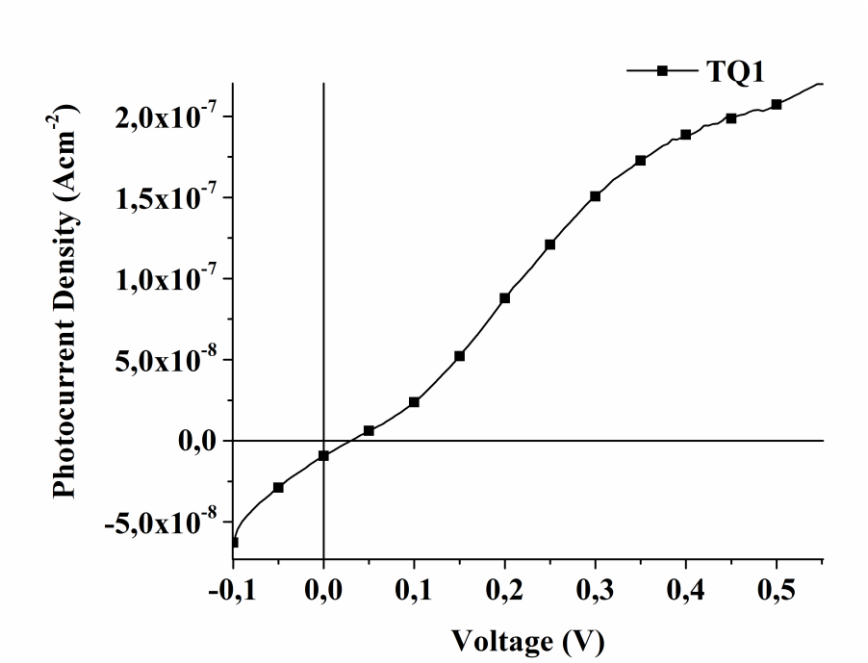

Figure S9. J-V curve of solar cell with TQ1 as the HTM. Almost no voltage and practically no current.

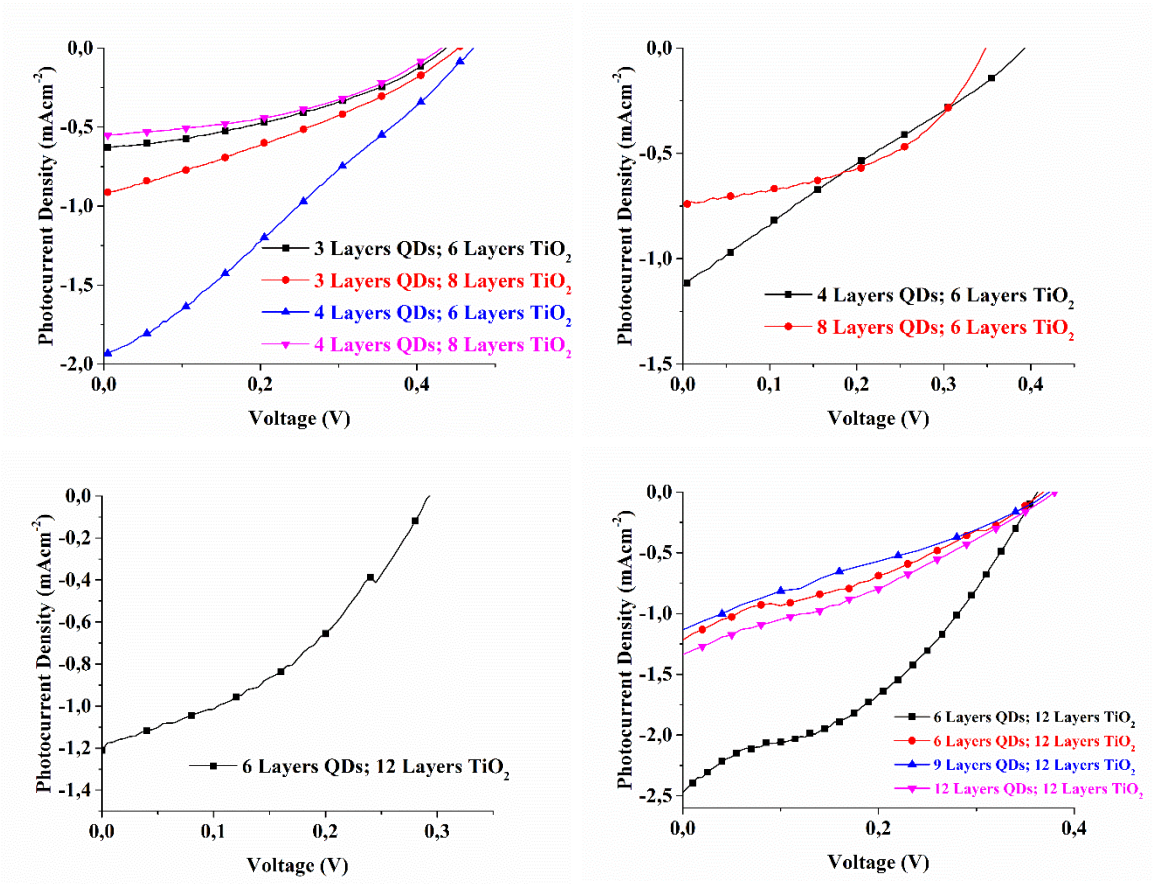

Figure S10. J-V-curves of several devices made by using Spiro-OMeTAD (a-c) and P3HT (d) as an HTM. The different cells in (a-c) are separated as they are made at different occasions. In (d), the 3 P3HT devices showing -1 to -1.5 mA/cm2 are made at a different occasion than the best device.

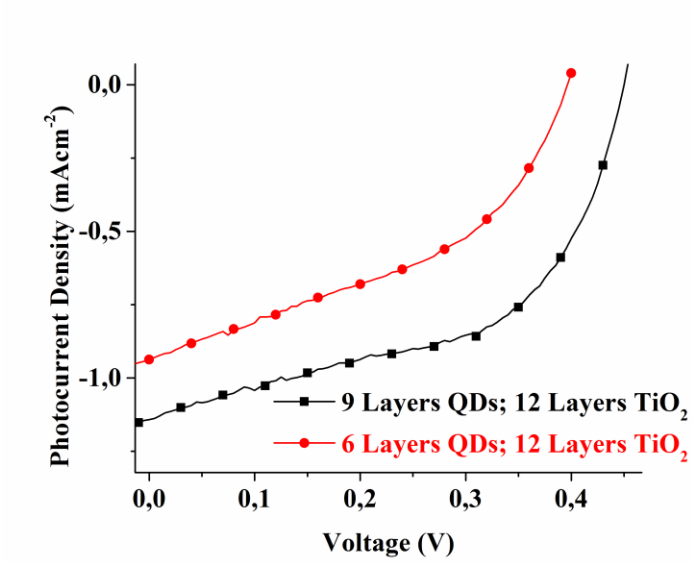

Figure S11. J-V-curves of the best devices using no HTM.

Table S2 – Non-rounded parameters of the best cell efficiencies.

HTM	*Voc* (V)	*Jsc* (mAcm-2)	FF	Efficiency (%)
Spiro-OMeTAD	0.47	-1.931	0.276103	0.250583
P3HT	0.365	-2.4709	0.377648	0.340593

None	0.45	-1.14198	0.519371	0.2669

References

1. Lu, L.; Zheng, T.; Wu, Q.; Schneider, A.M.; Zhao, D.; Yu, L. Recent advances in bulk heterojunction polymer solar cells. *Chem. Rev.* **2015**, *115*, 12666-12731, doi:10.1021/acs.chemrev.5b00098.
2. Ye, M.; Hong, X.; Zhang, F.; Liu, X. Recent advancements in perovskite solar cells: Flexibility, stability and large scale. *J. Mater. Chem. A* **2016**, *4*, 6755-6771, doi:10.1039/C5TA09661H.
3. Sveinbjornsson, K.; Aitola, K.; Zhang, J.; Johansson, M.B.; Zhang, X.; Correa-Baena, J.-P.; Hagfeldt, A.; Boschloo, G.; Johansson, E.M.J. Ambient air-processed mixed-ion perovskites for high-efficiency solar cells. *J. Mater. Chem. A* **2016**, *4*, 16536-16545, doi:10.1039/C6TA06912F.
4. Zhang, X.; Zhang, J.; Liu, J.; Johansson, E.M.J. Solution processed flexible and bending durable heterojunction colloidal quantum dot solar cell. *Nanoscale* **2015**, *7*, 11520-11524, doi:10.1039/C5NR02617B.
5. Bi, D.; Yang, L.; Boschloo, G.; Hagfeldt, A.; Johansson, E.M.J. Effect of different hole transport materials on recombination in CH3NH3PbI3 perovskite-sensitized mesoscopic solar cells. *The J. Phys. Chem. Lett.* **2013**, *4*, 1532-1536, doi:10.1021/jz400638x.
6. Etxebarria, I.; Ajuria, J.; Pacios, R. Solution-processable polymeric solar cells: A review on materials, strategies and cell architectures to overcome 10%. *Org. Electron.* **2015**, *19*, 34-60, doi:10.1016/j.orgel.2015.01.014.
7. Yan, J.; Saunders, B.R. Third-generation solar cells: A review and comparison of polymer: Fullerene, hybrid polymer and perovskite solar cells. *RSC Adv.* **2014**, *4*, 43286-43314, doi:10.1039/C4RA07064J.
8. Li, G.; Zhu, R.; Yang, Y. Polymer solar cells. *Nat Photon* **2012**, *6*, 153-161,
9. Ameri, T.; Min, J.; Li, N.; Machui, F.; Baran, D.; Forster, M.; Schottler, K.J.; Dolfen, D.; Scherf, U.; Brabec, C.J. Performance enhancement of the P3HT/PCBM solar cells through NIR sensitization using a small-bandgap polymer. *Adv. Energy Mater.* **2012**, *2*, 1198-1202, doi:10.1002/aenm.201200219.
10. Zhang, X.; Justo, Y.; Maes, J.; Walravens, W.; Zhang, J.; Liu, J.; Hens, Z.; Johansson, E.M.J. Slow recombination in quantum dot solid solar cell using p-i-n architecture with organic p-type hole transport material. *J. Mate. Chem. A* **2015**, *3*, 20579-20585, doi:10.1039/C5TA07111A.
11. Noh, J.H.; Jeon, N.J.; Choi, Y.C.; Nazeeruddin, M.K.; Gratzel, M.; Seok, S.I. Nanostructured TiO_2/$CH_3NH_3PbI_3$ heterojunction solar cells employing Spiro-OMeTAD/Co-complex as hole-transporting material. *J. Mater. Chem. A* **2013**, *1*, 11842-11847, doi:10.1039/C3TA12681A.
12. Alfred J. Frueh, J. The crystallography of silver sulfide, Ag_2S. *Zeitschrift für Kristallographie* **1958**, *110*, 136-144, doi:10.1524/zkri.1958.110.16.136.
13. Wang, E.; Hou, L.; Wang, Z.; Hellström, S.; Zhang, F.; Inganäs, O.; Andersson, M.R. An easily synthesized blue polymer for high-performance polymer solar cells. *Adv. Mater.* **2010**, *22*, 5240-5244, doi:10.1002/adma.201002225.